NIAC Final Report – Summary of Research
NASA Award NNX11AR40G

Steering of Solar Sails Using Optical Lift Force

Grover A. Swartzlander, Jr.
Rochester Institute of Technology

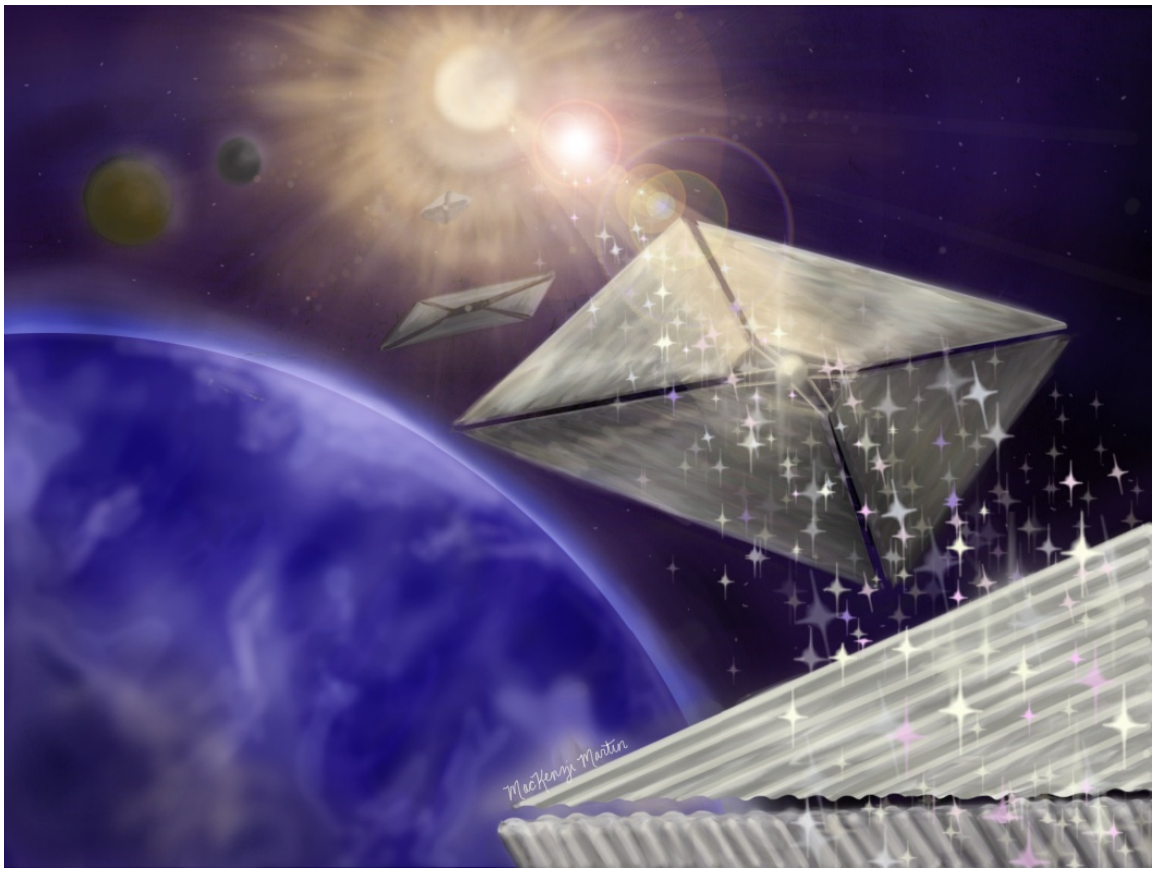

Acknowledgements

Alexandra Artusio-Glimpse, Rochester Institute of Technology, Rochester, NY
Alan Raisanen, Rochester Institute of Technology, Rochester, NY
Stephen Simpson, Univ. Bristol, UK
Charles (Les) Johnson, NASA Marshall Space Flight Center, Huntsville, AL
Andrew Heaton, NASA Marshall Space Flight Center, Huntsville, AL
Catherine Faye, NASA Langley, Langley, VA
John Dankanich, NASA Glenn, Cleveland, OH
Amy Davis, NeXolve Corp., Huntsville, AL

SUMMARY

Optical wing structures were theoretically and numerically analyzed, and prototype arrays of wings called optical flying carpets were fabricated with solar sail material clear polyimide (CP1). This material was developed at NASA Langley to better withstand damaging ultraviolet radiation found in outer space. Various optical wing sizes and shapes were analyzed to develop design strategies for thrust and torque applications. The developed ray-tracing model has undergone continual advancement, and stands as an effective tool for modeling most types of solar sails. To our understanding, such a model does not exist elsewhere. The distributed forces and torques have been reduced to a simple theoretical whereby the fundamental mechanics may be understood in terms of the numerically determined center of pressure offset from the center of mass. This description applies to any type of solar sail, affording our ray-tracing model a general utility. This research has established a foundation for understanding the force and torque afforded by optical wings. The study began by considering transparent wings and ended by considering wings having a reflecting face. The latter was found to afford the advantages of high thrust and both intrinsic and extrinsic torque. Our discovery of the intrinsic torque on optical wings (meaning that a moment arm is not required) has no analogy for a flat reflective solar sail, and therefore provides an extra degree of control that may be useful for sailcraft attitude and navigation purposes.

THEORETICAL

Radiation pressure is exerted on an object owing to the absorption or redirection of electromagnetic momentum. Redirected momentum is attributed to refraction, reflection, or re-emission of light. Assuming low loss, absorption and re-emission may be ignored. Numerical methods are required to determine the force and torque exerted on a refractive and/or reflective body of arbitrary shape. We have used both ray-tracing and wave-optics models to explore how basic elements, namely long cambered rods, are pushed and rotated when uniformly illuminated by a beam of light. Following examples found in aeronautics, we have developed the theory of radiation pressure in terms of an applied center of pressure, thereby reducing a complicated system to an elegant formalism.

Flat Reflecting Sail

It is instructive to first consider the force and torque exerted on a uniformly illuminated flat reflective sail, as illustrated in Fig. 1. Light directed along the x-axis ($\phi = \pi/2$, $\theta = 0$) The is incident on the surface at angles θ and ϕ, resulting in a force that is normal to the surface:

$$\bar{\mathrm{f}} = 2(IA/c)(\hat{n}\cdot\,\hat{x})^2\hat{n} \tag{1}$$

where $\hat{n} = \sin\phi\cos\theta\hat{x} + \hat{y}\sin\phi\sin\theta\hat{y} + \cos\phi\hat{z}$ is the unit normal vector of the surface of area A. The solar irradiance is given by $I = L/4\pi r^2$, where $L = 385\times x10^{24}$ [J/s] is the broad-spectrum solar luminous flux and r is the distance from the sun. At $r = 1\,[\mathrm{AU}] = 150\times\mathrm{x}10^{9}$ [m] the maximum value of solar pressure is $P_{\max} = 2I/c = 9.12\times10^{-6}$ [N/m^2]. This pressure is roughly four orders of magnitude greater than the solar wind pressure [McInnes 1999, p. 54]. For a sailcraft of total mass *m* and sail area *A*, the acceleration is given by $a = P/\sigma$, where $\sigma = m/A$ is the areal density. At 1 [AU] from the sun, the gravitational acceleration of the sun is $a_{sun} = GM/r^2 = 5.9$ [mm/s^2]. The sailcraft may experience an equal and opposite acceleration at an areal density $\sigma_0 = P/a_{sun} = 1.54$ [g/m^2].

Note that this value is independent of the distance from the sun, since both forces decrease inversely with the squared distance. From this gravitational point of view, the sailcraft acceleration may be expressed in terms of the "lightness" number $\beta = \sigma_0 / \sigma$, mass of the sun M_S, and gravitational const, G:

$$\vec{a} = (\beta G M_S / r^2)(\hat{n} \cdot \hat{x})^2 \hat{n} \tag{2}$$

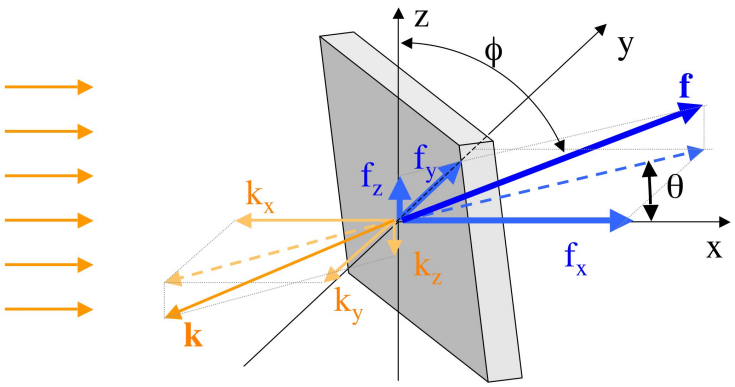

Figure 1. Light incident in the x-direction on a perfectly reflective surface. Reflected light produces a radiation pressure force in the direction **f**, normal to the surface.

Radiation Pressure on an Arbitrary Body

The net radiation pressure force on an arbitrary body may be expressed in terms of an efficiency vector, $\vec{Q}$ whose magnitude is $Q = 2$ for a perfect sun-facing sail ($\phi = \pi/2$, $\theta = 0$):

$$\vec{f} = (IA/c)\vec{Q} \tag{3}$$

Based on the conservation of momentum, we have determined that the optimal theoretical values of the longitudinal and transverse components of efficiency are given (assuming $\phi = \pi/2$) by

$$Q_{x,\text{opt}} = 1 - \cos(2\theta), \quad Q_{y,\text{opt}} = \sin(2\theta) \tag{4}$$

Figure 2 (left) shows these values plotted as a red circle, with the flat solar sail values plotted as a black ellipse. We note that our calculated optimal value predicts a transverse efficiency as large as $Q_y = 1$, whereas the flat sail can only achieve $Q_y = 0.77$. The latter occurs when $\theta \sim 35°$, $\phi = \pi/2$.

The x-component of force may be called the "forward scattering" or "thrust" component, whereas the y-component may be called the "lift" component. The word "lift" refers to a force in a direction perpendicular to the flow of incident light.

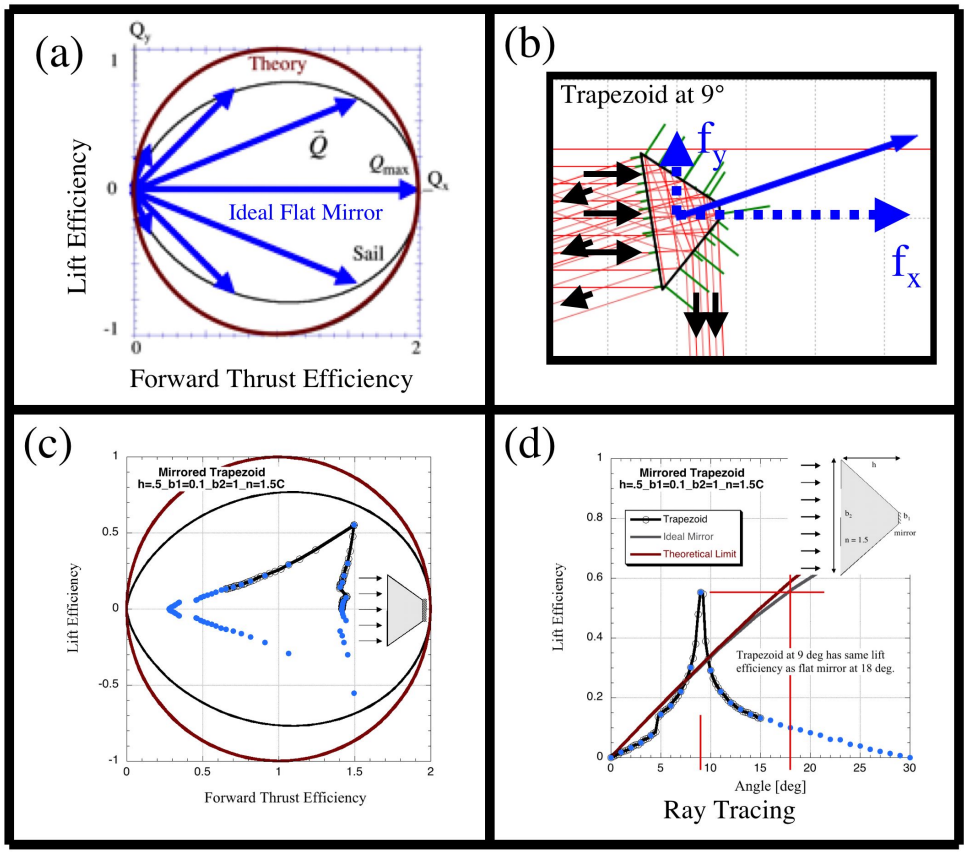

Figure 2. (a) Efficiency of radiation pressure force of a flat reflecting sail (blue arrows) does not achieve the theoretical limit (dark red circle) allowed by the conservation of momentum. (b) Ray tracing for a trapezoid, shown at an angle of attack of 9°. (c) Same at (a) but with the parametric efficiency curve for a trapezoid. (d) Lift efficiency as a function of angle of attack, showing lift values great than a flat reflector at 9°.

A flat reflective sail cannot reach the theoretical maximum lift efficiency owing to the factor cosθ that is attributed to the angle dependences of the sail cross-sectional area. That is, a tilted sail collects less light to reflect. This is depicted in Fig. 2(a). A solution to this problem would be to design the sail cross-section to be nearly sun-facing, while simultaneously deflecting the light perpendicular to the sun-line. This may allow the sail to perform at the physical limit (red line in Fig. 2 (a)). We considered various means to enhance the lift efficiency using single or arrayed optical wings. Although we found examples, such as the trapezoid in Fig. 2(b), where the lift force at a given angle of attack exceeded the lift force of a flat reflective sail at the same angle, we did not find examples exceeding the force vector ellipse, shown by the black line in Fig. 2 (a). For example, when a funnel-like trapezoid have a reflective smaller rear surface is placed in the beam, we predict a constant forward scattering force for angles of attack over the range ±9° (see Fig. 2(c)) where the forward thrust efficiency is ~1.5 while the lift efficiency varies from ±50%). What is more, this wing design provides more lift force than a comparable flat reflective sail, even though the trapezoid mirror surface is only 10% of that of a flat mirror. This means that the funnel-wing could (1) more readily provide maneuvering action than a flat mirrored surface, and (2) vary the lift force without affecting the forward scattering force. As this example illustrates, the shape of the wing may be tailored to suit a particular application over a range of orientation angles. As we explored only a narrow region of parameter space, e.g., varying the wing cross-sectional shape (see Fig. 3) and refractive index, the results in Fig. 2 suggest that greater optimization of large lift efficiencies is possible.

Controlling the lift force is an import component in the navigation of a sailcraft. For example, orbit-raising or orbit-lowering can be achieved by accelerating or decelerating the sailcraft along an orbital trajectory. Precise maneuvering of the craft may also be desired – for example, in a mission to encounter space debris, or to maintain a formation relative to other crafts. In many cases, it may be disadvantageous to tilt the entire sailcraft. Various mechanisms, such as motor-driven tip vanes, and actuated ballast mass have been proposed to achieve fine-scale attitude control. Here we have explored the feasibility of using optical wings to lift and torque a sailcraft.

An optical wing is an analog to an airfoil. It is a long structure having a cambered cross-section. Examples of optical wings are shown in Fig. 3. In this study we assume the wings have a length greater than other dimensions, therefore reducing the problem to two dimensions. We also assume they are composed of a non-absorbing homogenous, isotropic dielectric material of refractive index *n*. In some cases we allow for a reflective coating on one of the facets.

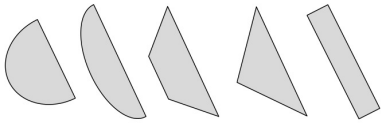

Figure 3. Example of optical wing cross-sections. Bodies may be refractive with optional reflective coatings over selected facets.

The radiation pressure force and torque on such bodies will depend on the orientation or "angle of attack" relative to the incident beam of light. Force and torque plots are discussed in the Numerical section. Here we discuss the mechanics of the wing for an arbitrary value of force and torque. In general the "center of pressure" (cp) will be offset from the center of mass (cm), causing the body to rotate. If the net force and torque is known at a given angle of attack, the center of pressure $\vec{r}_{cp}$ is found by satisfying the expressions:

$$\vec{r}_{cp} \times \vec{f} = \vec{T}, \quad \vec{r}_{cp} \cdot \vec{f} = 0 \tag{5}$$

Figure 4 depicts the centers of mass and pressure for a uniformly illuminated glass rod have a semicircular cross-section. In this diagram, the wing has a scattering force (in the direction of the incident rays), an upward lift force, and a torque that rotates the body clockwise. As shown in the right hand side of Fig. 4, the wing can assume different trajectories when the initial orientation is not in a rotationally stable equilibrium state.

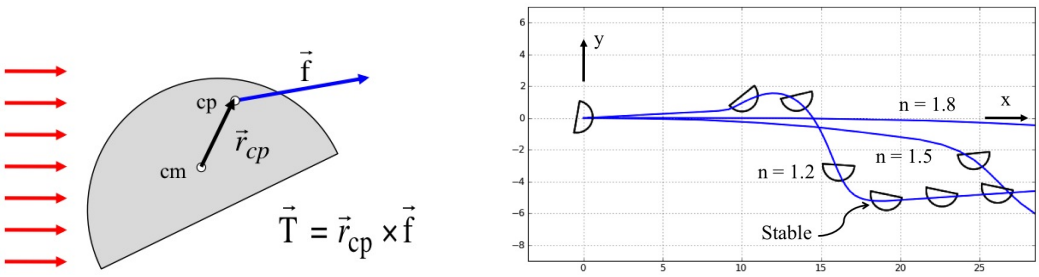

Figure 4. Left: Illustration of displaced centers of mass and pressure. At this instant in time the body rotates clockwise and accelerates upward and to the right. Right: Examples of the particle trajectory and orientation in a viscous medium for three different values of the refractive index of the wing.

If we desire torque-free forces, clearly the wing must operate at or near a position of stable rotational equilibrium. As suggested by Eq. (5), this can occur when the center of pressure vector is parallel to the force vector (i.e., the line of force intersects the center of mass), or when the displacement between the centers of mass and pressure are vanishingly small. To determine the stable rotational equilibrium positions, we must use numerical modeling, as analytical methods do not exist for this task. Examples of such modeling is described in the next section.

In a zero-damping environment such as free space, an optical wing may rotationally oscillate about an equilibrium angle: $\Delta\theta(t) = \theta(t) - \theta_{eqlm} \approx \Delta\theta_0 \cos(\omega t)$, assuming a Hooke's law restoring torque: $T \approx -k\Delta\theta$ for small values of $\Delta\theta_0$. By actively driving the oscillations in a feedback loop, one may increase or decrease the amplitude of oscillation, $\Delta\theta_0$. The frequency of oscillation is determined by the torsional stiffness, *k*, and the moment of inertia, I_{wing}: $\omega = \sqrt{k / I_{wing}}$. From considerations of the torque about the edge of a flat mirror, we predict this frequency to roughly scale as $\omega_0 = \sqrt{IL/cm} = \sqrt{I/c\rho A}$ where *A* and ρ are the cross-sectional area and mass density of the wing, respectively. For example, if I = 1 [kW/m^2], ρ = 1g/cm^3 = 10^3 kg/m^2 then $\omega_0 = \sqrt{(1/3)10^{-8}[m^2/s^2]A}$ (see plot in Fig. 5).

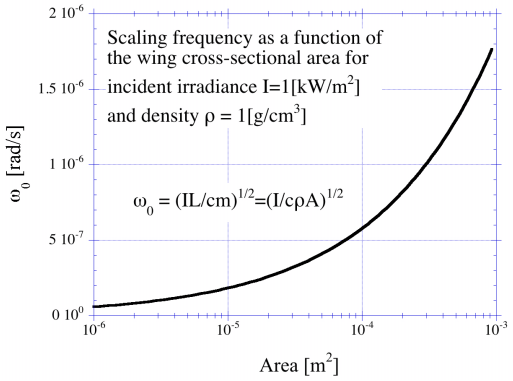

Figure 5. Frequency scaling as a function of an optical wing oscillator of cross-sectional area A.

Once the torque and force are numerically determined for all possible angles of attack, the orientation and linear positions may be determined by numerical integration (e.g., 4th order Runge-Kutta):

$$\begin{aligned} \theta(t-t_0) &= \theta_{t0} + \dot{\theta}_{t0}\cdot(t-t_0) + (1/2)\ddot{\theta}(t-t_0)^2 \\ x(t-t_0) &= x_{t0} + \dot{x}_{t0}\cdot(t-t_0) + (1/2)\ddot{x}(t-t_0)^2 \\ y(t-t_0) &= y_{t0} + \dot{y}_{t0}\cdot(t-t_0) + (1/2)\ddot{y}(t-t_0)^2 \end{aligned} \qquad (6)$$

where $\ddot{\theta} = T / I_{wing}$, $\ddot{x} = f_x / m$, and $\ddot{y} = f_y / m$. (Note that we have considered the two-dimensional case whereby other degrees of freedom are ignored.) The numerically determined phase diagram for the angle of attack, θ, and the angular velocity, $\dot{\theta}$, is shown in Fig. 6 for a semicircular wing having the flat side coated with a mirror. Note the wide range of angles (±50°) over which the wing may rock back and forth. The closed orbits in Fig. 6 may be made to spiral inward by synchronously illuminating or

shuttering the light reaching the wing. A detailed report on oscillating optical wings is included in the supplementary material, "Refractive optical wing oscillators with one reflective surface."

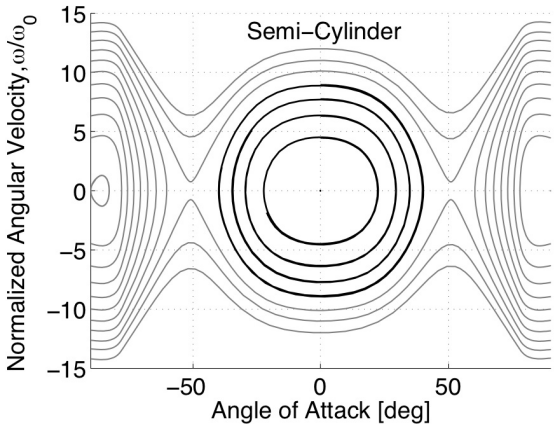

Figure 6. Phase diagram showing periodic (dark lines) rocking motion of a semicircular wing with a reflective flat side.

When any of the dimensions of the wing approaches, or becomes less than the wavelength of light, the ray-tracing model must be replaced with a wave optics model. This is necessary because interference phenomena may dominate the optical field. Further, the concept of a ray cannot be applied for cases where the optical field varies over such short distance scales. See supplementary material "Optical lift from dielectric semicylinders".

The net radiation pressure force and torque on an optical wing may be found by numerically summing over a large number of rays refracted and reflected from the surface:

$$\mathbf{f} = \sum \mathbf{f}_i, \quad \mathbf{T} = \mathbf{T}_{ex} + \mathbf{T}_{in} : \quad \mathbf{T}_{ex} = \mathbf{r}_0 \times \mathbf{f}, \quad \mathbf{T}_{in} = \sum \mathbf{r}_i \times \mathbf{f}_i \tag{7}$$

where $\mathbf{T}_{ex}$ and $\mathbf{T}_{in}$ are respectively the extrinsic and intrinsic torque, $\mathbf{r}_0$ is a moment arm from the origin to the center of mass, and $\mathbf{r}_i$ is a vector pointing from the center of mass of the wing to the surface where a ray produces a force, $\mathbf{f}_i$. The intrinsic may arise when the center of mass and center of pressure are offset, e.g., when the wing is not at a position of stable rotation equilibrium. Note that intrinsic torque is zero valued for a flat rectangular reflective sail. Optical wings therefore provide a distinct new component of attitude control for solar sails. For example, an array of *N* wings (i.e., an optical flying carpet) may feel no extrinsic torque, but a multiplicative intrinsic torque. That is:

$$\mathbf{T}_{ex,net} = \sum_{j=1}^{N} (\mathbf{r}_{0,j} \times \mathbf{f}_j) = 0, \qquad \mathbf{T}_{in,net} = \sum_{j=1}^{N} \sum \mathbf{r}_{i,j} \times \mathbf{f}_{i,j} = N\mathbf{T}_{in} \tag{8}$$

For an array of semicircular optical wings having a reflective flat side, the intrinsic torque will provide a restoring torque. This may be particularly advantageous for a sun-facing solar sail mission such as a solar weather station at a sub-Lagrange point. By matching the rocking period of the sail to the period of the halo orbit, no fuel or mechanical parts would be needed to maintain a sun-facing orientation. Active electro-optic control methods may be used to increase or decrease angular excursions.

EXPERIMENTAL

The first experimental realization of optical lift was demonstrated with single semi-cylindrical wings. This shape was selected for early investigations of optical lift because the semicircular profile is a simplified cambered shape. Our ray-tracing computer model indicates that other wing shapes will experience optical lift and stable lift orientations when exposed to uniform illumination. The first new wing shape to be fabricated was the rectangular rod, followed by arrays of joined semi-cylindrical wings. These two objects were fabricated using photolithographic techniques. The discussed fabrication methods produced these objects with expected regularity and only minor shape artifacts. Early tests of the rectangular optical wing indicated good agreement with computer model predictions.

Following similar methodology as in the fabrication of semi-cylindrical optical wings, the new rectangular wings were made of patterned photoresist using photolithography. This process began with a 1.5μm thick layer of OiR 620 positive photoresist spin-coated onto a blank silicon wafer. OiR 620 photoresist was selected for its common use in photolithography with a refractive index of 1.6. The resist was then exposed to UV illumination with a GCA Stepper through a mask that defined the two-dimensional length and width of each wing in an array of many sizes (see background image in Fig. A). The exposed wafer was then developed to wash away excess resist, and baked on a hot plate to further solidify the resist particles. Finally, the surface of the silicon was etched in xenon hexafluoride (XeF6) for 10 hours. This released the photoresist particles, which were then collected with a surfactant-water bath.

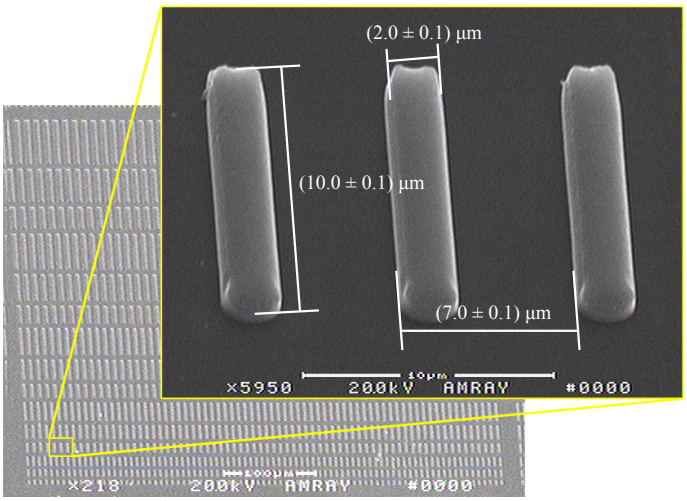

Figure A - SEM images of rectangle optical wings. Background image shows one set of wings increasing in size from the bottom of the image to the top. A sub-region is enlarged showing three 10 μm x 2 μm wings with measurements and spacing.

These fabricated rectangular were tested in a simple apparatus for determining the optical lift force incident on these objects. The submerged particles were placed in a well that was illuminated from below with a 42mW, 975nm, collimated laser beam with a diameter of 50μm. The particles were imaged through a 40x objected by a video camera such that any transverse movements of an illuminated particle were recorded. This testing indicated that the wing rotated into a stable angle of attack at roughly 50° with an approximate lift force of 3.4 pN. The same wing parameters from Fig. A were inputted into the computer model to recreate the force and torque that this particle experienced. The computer model determined that this wing rotates into a stable orientation at 54° above the horizontal as shown in Fig. B. At this stable position, the lift angle (angle corresponding to the transverse component of total force on the object) is 30°. The model predicts a lift force of 4.6pN in an ideal liquid; however, in a real fluid the force would be expected to be less than this ideal case. These computer-modeling results indicate good agreement with the tested wing.

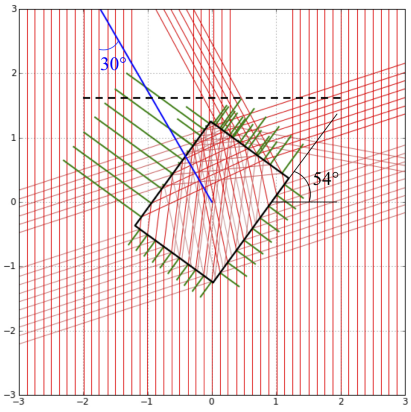

Figure B – Two-dimensional ray plot of rectangular wing from Fig. A generated by computer model. Red light rays are traveling upwards and are incident on the wing producing a total force given by the blue line. Black dashed-line is an approximation to the plane imaged by the video camera.

Several iterations have been implemented in the early fabrication stages of arrays of semi-cylindrical wings. These arrays are fabricated using isotropic reactive ion etching (RIE) to form a silicon mold. In the first trial of this fabrication technique, the mold was filled with a PDMS polymer (silicone elastomer) that was lifted from the mold by hand. This is a hydrophobic polymer with a refractive index of about 1.4. The elastomer was selected because it may be spin coated onto the silicon mold, is easily cured, and is easily managed all at low cost.

To make the silicon mold using the isotropic RIE technique a 1μm layer of thermal silicon dioxide was first grown on a silicon wafer. The oxide was then patterned with OiR 620 resist using photolithography leaving holes of exposed oxide with a range of feature sizes. Then the oxide was etched down in buffered oxide etch (BOE) for 9 minutes using the patterned resist as a mask. This exposed areas of the silicon wafer below. To achieve isotropic profiles in the silicon, the silicon was etched in the Drytek Quad with sulfur hexafluoride (SF6) using resist over oxide as an etching mask. In the first test of this process, three iterations of the Drytek etching step were implemented with different exposure times - 10, 15, and 20 minutes - all at 240 W of power, 60 mTorr of pressure, and 20 sccm of gas flow. The resist on top the oxide was cleared away in this step, and the remaining oxide was then removed again in BOE for 10 minutes leaving behind a clean silicon mold with arrays of wells. Lastly, the mold was filled with PDMS. The wafer was then degassed for 30 minutes, baked on a hot plate at 70° Celsius for 3.5 hours, and allowed to rest over night before it was peeled off the silicone substrate by hand. The process is pictorially described in Fig. C where CP1 (Colorless Polyimide 1) has taken the place of the PDMS elastomer.

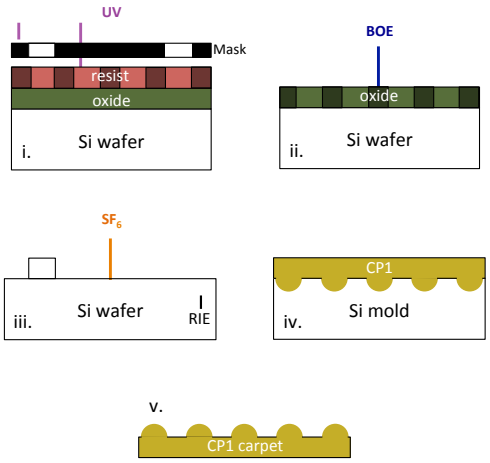

Figure C – Pictorial description of steps in fabrication of silicon mold for making semi-cylindrical wing arrays.

In the first trial with PDMS, the RIE technique did generate curved features in the silicon wafer, but the degree of curvature was small relative to the width of the features. This is due to aspect ratio dependent etching (ARDE), meaning much longer etch times would be needed to achieve semicircular profiles of this size. Smaller features are easily fabricated by the RIE process, but larger features require very long etch times that would destroy the oxide mask as occurred with the 20 minute wafer. In demolding the PDMS carpets, the polymer partially adhered to the silicon wafer, tearing the carpets, and leaving a spotty residue on the silicon.

After the first trial which produced oversized features as discussed, we successfully fabricated 180µm x 300µm x 370µm thick carpets with semi-cylindrical features that are 180µm long, 30µm wide, and 50µm tall. Fig. D below is a microscopic image of a silicon elastomer carpet. Though inexpensive and easy to work with, silicon elastomer is not a good material for fabrication of flying carpets because it is difficult to thin the substrate to less than 50µm and because the material breaks with defects as seen in Fig. D. At the first NAIC meeting, a chemist from NASA Langley informed us of the LARC-CP1 polyimide developed for solar sails. This material is more favorable for the fabrication of flying carpets because it is ultra-lightweight. It too may be spun onto the mold and released by hand.

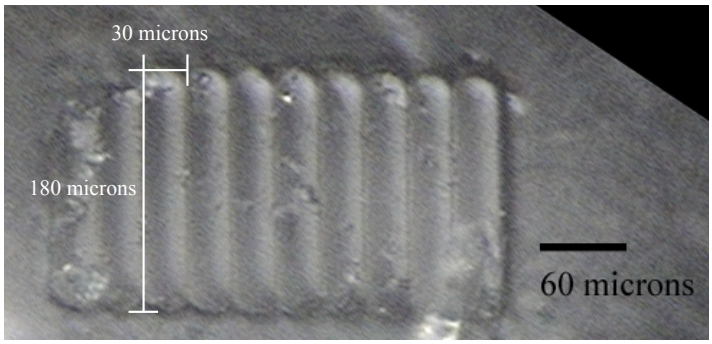

Figure D – 50x microscopic image of the smallest fabricated flying carpet mad out of silicon elastomer. Defects in the semi-cylindrical features are due to tearing of the elastomer while releasing it from the mold.

The first successful fabrication of a wing array made from CP1 was achieved near the end of the Phase I project. A 20x microscope image of these arrays on a 50 µm substrate is given in Fig. E. In addition before the end of the Phase I project, we designed a specialized mask for carpets including 1 cm^2, 1 mm^2, and 500 ¥ m^2 linear arrays of 20 ¥ m and 40 ¥ m long semi-cylindrical rods with 10 and 20 µm radii.

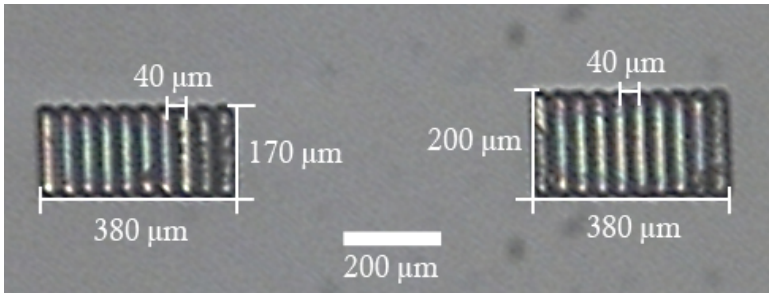

Figure E – 20x microscope image of first fabrication of CP1 arrays of semi-cylindrical wings on top a 50 mm substrate with 20 mm radii.

At the end of the Phase I project, two fabrication goals were set: 1) to decrease the substrate thickness of the CP1 arrays by improving the recipe for spin coating the resin onto the silicon mold, and 2) to fabricate single wings and arrays with mirrored back surfaces. A proposed recipe for the fabrication of these mirrored wing arrays is given in Fig. F.

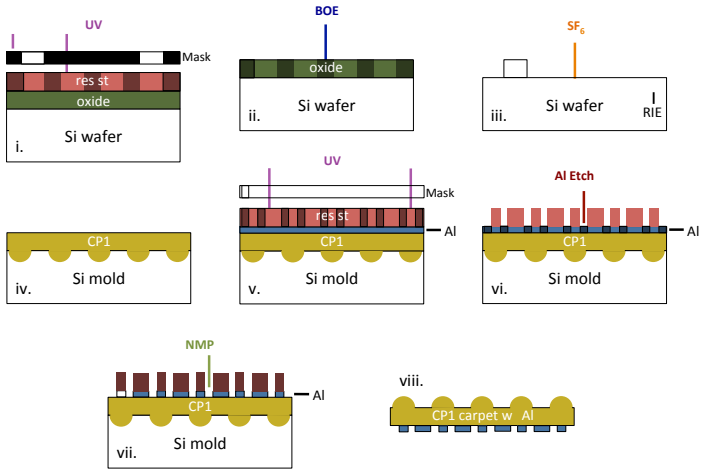

Figure F – Fabrication of mirrored wing arrays follows the same steps as were done for non-mirrored arrays with the addition of a second photoresist patterning of aluminum that would be sputtered onto the back side of CP1 substrate before releasing from the mold. Al etch would be done in a 16:1:1:2 bath of Nitric Acid, Acetic Acid, Phosphoric Acid and water, and excess resist would be removed in NMP (1-Methyl-2-pyrrolidon) solvent.

BIBLIOGRAPHY

Alhorn, D.C. and Scheierl, J.M., "FeatherSail – Design, Development and Future Impact," *NASA Technical Reports Server*, NASA, 3 May 2010. Web. 25 April 2011. <ntrs.nasa.gov/archive/nasa/casi.ntrs.nasa.gov/20100024167_2010023656.pdf>

Solar Sail Roadmap Mission GN&C Challenges, Andrew F. Heaton (NASA Marshall Space Flight Center), American Institute of Aeronautics and Astronautics

Kare, J. T., "High-acceleration Micro-scale Laser Sails for Interstellar Propulsion," *NIAC*, Universities Space Research Association, 31 December 2001. Web. 27 April 2011. <http://www.niac.usra.edu/files/studies/final_report/597Kare.pdf>

Landis, G.A., "Advanced Solar- and Laser-pushed Lightsail Concepts: Final Report," *NIAC*, Universities Space Research Association, 31 May 1999. Web. 27 April 2011. <http://www.niac.usra.edu/files/studies/final_report/4Landis.pdf>

Mulser, P. "Radiation pressure on macroscopic bodies," *J. Opt. Soc. Am. B* 2, 1814-1829 (1985).

Spieth, D., Zubrin, R, "Ultra-Thin Solar Sails for Interstellar Travel: Phase I Final Report," *NIAC,* Universities Space Research Association, December 1999. Web. 27 April 2011. <http://www.niac.usra.edu/files/studies/final_report/333Christensen.pdf>

Vulpetti, G., Johnson, L., Matloff, G.L., *Solar Sails: A Novel Approach to Interplanetary Travel*, Copernicus Books, Praxis Publishing (2008).

Vulpetti, G., "Total solar irradiance fluctation effects on sailcraft-Mars rendezvous," *Acta Astronautica* **68**, 644–650 (2011).

JAXA Press Release, "Small Solar Power Sail Demonstrator 'IKAROS' Successful Attitude Control by Liquid Crystal Device," 23 July 2010.

"NanoSail-D Latest News," www.nasa.gov/mission_pages/smallsats/nanosaild.html

Seeking a Human SpaceFlight Program Worthy of a Great Nation, NASA (2009).

Stepping-Stones to the Future of Space Exploration: A Workshop Report, National Academic Press (2004).

"Targets met for the Solar Sail IKAROS," www.scienceknowledge.org/2011/02/05/targets-met-for-the-solar-sail-ikaros

The Vision for Space Exploration, NASA (2004).

Coulter, D., and Phillips, T., "A Brief History of Solar Sails," Science @ NASA [online database], URL: http://science.nasa.gov/headlines/y2008/31jul_solarsails.htm (cited 15 December 2009).

Darling, D., "Solar Sail," The Internet Encyclopedia of Science [online database], URL: http://www.daviddarling.info/encyclopedia/S/solar_sail.html (cited 15 December 2009).
Friedman, L. D., "Projects: LightSail - The Future of Solar Sailing LightSail: A New Way and a New Chance to Fly on Light," The Planetary Society [online article], http://www.planetary.org/programs/projects/solar_sailing/tpr_lightsail.html (cited 25 March 2010).
Leary, W., "Into Orbit (Maybe Beyond) on Wings of Giant Solar Sails" New York Times, online, (21 June 2009).
Overbye, D., "Setting Sail Into Space Propelled by Sunshine," New York Times, online, (9 November. 2009).
Pappa, R., Lassiter, J., and Ross, B., Structural Dynamics Experimental Activities in Ultra- Lightweight and Inflatable Space Structures, NASA TM-2001-210857, (2001).
Scheierl, J. M. and Alhorn, D. C., Solar Sails: Design and Future Impact, NASA/MSFC/USRP Fall 2009 Intern Research Paper, Huntsville, AL (December 2009).
Stanford, N., "Hoisting the Solar Sail," Chemistry World [online database], URL: http://www.rsc.org/chemistryworld/Issues/2009/July/HoistingTheSolarSail.asp (cited 15 December 2009).
Swartzlander, G.A. Jr., Peterson, T. J., Artusio-Glimpse, A. B., and Raisanen, A. D., "Stable Optical Lift," *Nature Photonics* 5, 48-51 (2011).
Whorton, M. S, Heaton, A., Pinson, R., Laue, G., Adams, C., "NanoSail-D: The First Flight Demonstration of Solar Sails for Nanosatellites," AIAA/USU 22nd Conference on Small Satellites, SSC08-X-1, (August 2008).